Austin Chemical Engineering

Open Access

Austin Publishing Group

Review Article

# Molecular Docking, IR, Raman Studies on Heterocyclic Aromatic Compound

**Uma Maheswari J[1]* and Tom Sundius[2]**

[1]Department of Physics, Theivanai Ammal College for Women,Villupuram,India

[2]Department of Physics, University of Helsinki, Finland

***Corresponding author:** Uma Maheswari J, Department of Physics, Theivanai Ammal College for Women,Villupuram, Tamil Nadu, India

**Received:** March 04, 2015; **Accepted:** June 03, 2015; **Published:** June 06, 2015

**Abstract**

Quantum chemical calculations of energies, geometrical structure and vibrational wave numbers of clioquinol were carried out by DFT (B3LYP) method with 6-21G (d) basis set. The Fourier-Transform Infrared and Fourier-Transform Raman spectra of clioquinol were recorded in the region 4000-400 cm-1 and 3500-100cm-1. A detailed interpretation of the vibrational spectra of this compound has been made on the basis of the calculated Potential Energy Distribution (PED). Comparison of the simulated spectra with the experimental spectra provides important information about the ability of the computational method to describe the vibration mode. A molecular docking study was performed and the results indicate for the future drug designing. Ramachandran plot supports the docking studies by providing the ψ and Φ values for an amino acid in a protein.

**Keywords:** FT-IR; FT-Raman; Molecular docking; Topology; PED; Ramachandran plot

## Introduction

Iodochlorhydroxyquin (clioquinol) is an antifungal drug and antiprotozoal drug. It is neurotoxic in large doses. It is a member of a family of drugs called hydroxyquinolines which inhibit certain enzymes related to DNA replication. The drugs have been found to have activity against both viral and protozoal infections [1]. A result at UCSF indicates that clioquinol appears to block the genetic action of Huntington's disease in mice and in cell culture [2]. Evidence from phase 2 clinical trials suggested that clioquinol could halt cognitive decline in Alzheimer's disease, possibly owing to its ability to act as a chelator for zinc and copper ions. This led to development of analogs including PBT2 as potential therapeutic compounds for the treatment of Alzheimer's disease [3]. Literature says [3] that clioquinol acts directly on a protein called clock-1 and might slow down the aging process. Recent studies provides strong evidence that clioquinol is able to target tumor proteasome *in vivo* in a copper-dependent manner, resulting in formation of an active AR inhibitor and apoptosis inducer that is responsible for its observed antiprostate tumor effect [4]. Di chen *et al.* reported that clioquinol was capable of binding copper and forming a complex as verified by XANES and EXAFS. Biochemical analysis revealed that clioquinol induced cancer cell death through apoptotic pathways that require caspase activity. It has anticancer effects both *in vitro* and *in vivo* [5].

Knowledge of drug-biomolecules interactions contributes to a better understanding of the transportation, metabolism, and toxicity of drugs at molecular level. Spectroscopic methods are powerful tools in coping with problem of molecular mechanisms with advantages of simplicity, rapidity and high sensitivity [6-8]. Quantum chemical computational methods have proved to be an essential tool for interpreting and predicting the vibrational spectra [9,10]. Now a days, sophisticated electron correlation and density functional theory calculations are increasingly available and deliver force field of high accuracy even for large polyatomic molecules [11,12]. Density Functional Theory calculations of vibrational spectra of many organic systems [13-16] have shown promising conformity with experimental results and they provide excellent vibrational frequencies of organic compounds if the calculated frequencies are scaled to compensate for the approximate treatment of electron correlation, for the basis set deficiencies and for the anharmonicity [17-19]. Molecular docking was further employed to find the ligand sites of clioquinol to understand the interaction. Knowledge about the site at which a ligand binds provides an important clue for predicting the function of a protein and is also often a prerequisible for performing docking

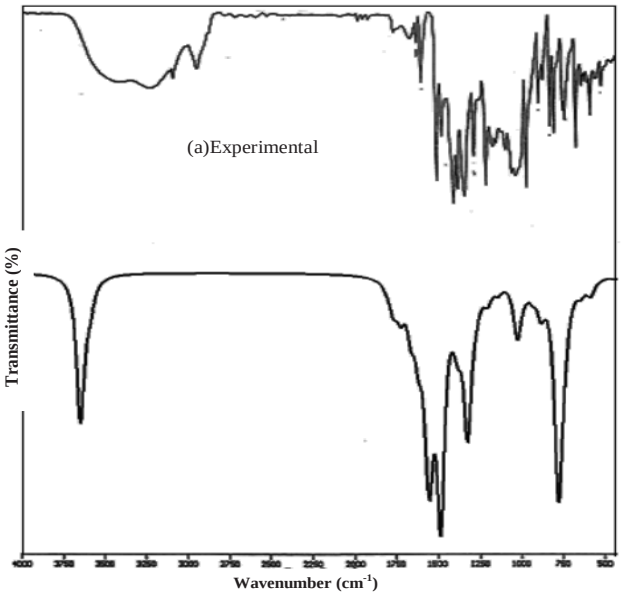


**Figure 1:** FT-IR spectra of Clioquinol (Experimental/theoretical).




**Citation:** Maheswari JU and Sundius T. Molecular Docking, IR, Raman Studies on Heterocyclic Aromatic Compound. Austin Chem Eng. 2015;2(1): 1016.

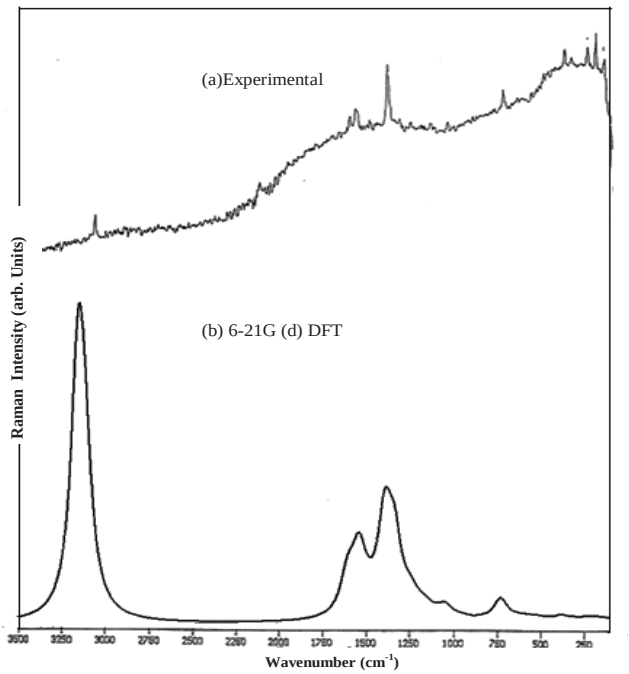


**Figure 2:** FT-Raman spectra of Clioquinol (Experimental/ theoretical).

computations in virtual drug design and screening. The aim of the present study is to give a complete description of the molecule geometry and molecular vibrations of the title molecule. For that purpose, quantum chemical computations were carried out for clioquinol using DFT method. These calculations are valuable for providing insight into the vibrational spectrum and molecular parameters is expected to be helpful in evaluating the potential of clioquinol to environment and human health.

### Experimental

The compound clioquinol in the solid form was obtained from the Sigma-Aldrich chemical company with a stated purity of 98% and used as such without further purification. The FTIR and FT-Raman spectra of the sample were recorded in the region 4000-400 $cm^{-1}$ and 3500-100 $cm^{-1}$ respectively using BRUCKER IFS 66V FTIR spectrometer with a resolution of 0.5 $cm^{-1}$ at RSIC, Chennai, India. All the sharp bands of the spectrum have an accuracy of ± 1$cm^{-1}$. The experimental and simulated FTIR and FT-Raman spectra are shown in Figure 1 and 2.

### Computational details

All calculations were performed using the G03W [20,21] software. Initial geometry generated from standard geometrical parameters [22] and full optimizations were carried out. The vibrational wavenumbers, geometric parameters, and other molecular properties were carried out using DFT (B3LYP) method with 6-21G (d). To compensate for the errors arising from basis set incompleteness and neglect of vibrational anharmonicity, we have scaled the wave numbers with scaling factors. All the parameters were allowed to relax and the calculations converged to an optimized geometry which corresponds to a true minimum, as seen from the lack of imaginary wave numbers. The Cartesian representation of the theoretical force constants has been computed at the fully optimized geometry. Transformation of

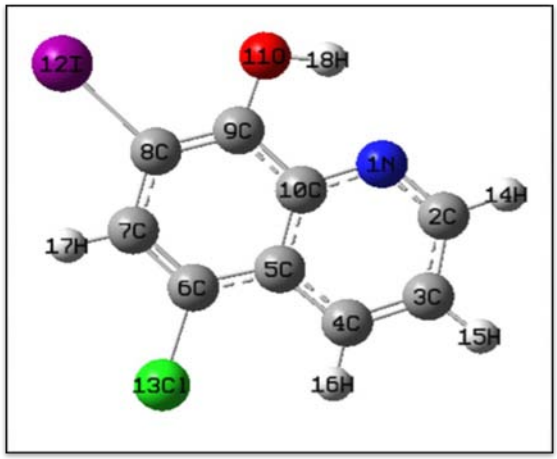


**Figure 3:** Numbering system adopted Clioquinol.

force field, the subsequent normal coordinate analysis and calculation of the Potential Energy Distribution (PED) were done on a PC with the MOLVIB program (version V 7.0) written by Sundius [23]. The Natural Bond Orbital (NBO) analysis were performed using NBO 3.1 program as implemented in the Gaussian 03W package at the above said level.

## Results and Discussion

### Geometrical structure

The optimized structure parameters for the clioquinol are calculated by DFT (B3LYP) with 6-21G (d) basis set. The labeling of atoms for clioquinol is given in Figure 3. Comparison table for the calculated bond lengths and angles for clioquinol with those of experimentally [24] available x-ray diffraction data are listed in the Table 1. From the theoretical values, we can find that most of the optimized bond angles are slightly larger than the experimental values, due to the theoretical calculations belong to the molecules in gaseous phase and the experimental results belong to the molecules in solid phase. Comparing bond angles and lengths as a whole, the values of B3LYP correlates well compared with the experimental results. Inspite of the differences calculated geometric parameters represent a good approximation and they are the bases for calculating other parameters such as vibrational frequencies.

### Topology analysis

Ring count=2

Ring atom count=10

Ring bond count =11

Aromatic ring count=2

Aliphatic atom count=3

Aliphatic bond count=3

Aromatic atom count=10

Aromatic bond count=11

Carbo ring count=1

Hetero ring count=1

**Table 1:** Optimized parameters for Clioquinol B3LYP with 6-21G (d).

| Parameters | Experimental[a] | B3LYP/ 6-21G(d) |
|---|---|---|
| **Bond length** | | |
| N(1)-C(2) | 1.35 | 1.32 |
| N(1)-C(10) | 1.35 | 1.36 |
| C(2)-C(3) | 1.42 | 1.41 |
| C(2)-H(14) | 1.1 | 1.08 |
| C(3)-C(4) | 1.42 | 1.37 |
| C(3)-H(15) | 1.1 | 1.08 |
| C(4)-C(5) | 1.42 | 1.41 |
| C(4)-H(16) | 1.1 | 1.08 |
| C(5)-C(6) | 1.42 | 1.42 |
| C(5)-C(10) | 1.42 | 1.42 |
| C(6)-C(7) | 1.42 | 1.37 |
| C(6)-Cl(13) | 1.71 | 1.76 |
| C(7)-C(8) | 1.42 | 1.41 |
| C(7)-H(17) | 1.1 | 1.08 |
| C(8)-C(9) | 1.42 | 1.37 |
| C(8)-I(12) | 2.14 | 2.12 |
| C(9)-C(10) | 1.42 | 1.42 |
| C(9)-O(11) | 1.33 | 1.35 |
| O(11)-H(18) | 0.97 | 1.01 |
| **Bond Angle** | | |
| C10-N1-C2 | 114.99 | 118.49 |
| C3-C2-N1 | 123.5 | 122.34 |
| H14-C2-N1 | 116.50 | 117.33 |
| C5-C10-N1 | 120.00 | 123.32 |
| H14-C2-C3 | 120.00 | 120.31 |
| C4-C3-C2 | 129.38 | 119.62 |
| H15-C3-C2 | 120.00 | 119.53 |
| H15-C3-C4 | 120.00 | 120.84 |
| C5-C4-C3 | 115.61 | 119.64 |
| H16-C4-C3 | 122.19 | 121.14 |
| H16-C4-C5 | 122.19 | 119.20 |
| C6-C5-C4 | 119.99 | 125.96 |
| C10-C5-C4 | 120.00 | 116.56 |
| C10-C5-C6 | 119.99 | 117.46 |
| C7-C6-C5 | 120.00 | 120.80 |
| C5-C10-C9 | 119.99 | 121.54 |
| Cl13-C6-C7 | 120.00 | 119.36 |
| C8-C7-C6 | 119.99 | 120.48 |
| H17-C7-C6 | 120.00 | 119.73 |
| H17-C7-C8 | 120.00 | 119.27 |
| C9-C8-C7 | 119.99 | 120.48 |
| I12-C8-C7 | 120.00 | 120.54 |
| I12-C8-C9 | 120.00 | 118.97 |
| C8-C9-C10 | 119.99 | 118.70 |
| O11-C9-C8 | 124.30 | 123.62 |
| O11-C9-C10 | 124.30 | 117.66 |
| H18-O11-C9 | 108.00 | 104.83 |

[a]Ref: [24]

Hetero aromatic ring count=1

Carbo aromatic ring count=1

Fused aromatic ring count=2

## Vibrational assignments

IR and Raman spectra contain a number of bands at specific wavenumbers. The aim of the vibrational analysis is to decide which of the vibrational modes give rise to each of these observed bands. According to the theoretical calculations, clioquinol has a structure of $C_1$ point group has 18 atoms and 48 modes of fundamental vibrations. The Table 2 shows. FT-IR and FT-Raman frequencies assignments for clioquinol. The potential energy distributions are also supporting the present study. The computed intensities show marked deviations from the observed values. One may note that the computed wavenumbers correspond to the isolated molecular state, whereas the observed wavenumbers correspond to the solid state spectra. We have assigned the fundamental mode of clioquinol on the basis of a group vibrational concept and calculated vibrational wavenumbers. On the whole, the predicted vibrational wavenumbers are in agreement with the experimental results. The internal coordinates and symmetry coordinates are given in Table 2 and Table 3. The resultant scaled frequencies, measured infrared, Raman band positions and their assignments are presented in Table 4. The internal coordinates describe the position of the atoms in terms of distances, angles and dihedral angles with respect to an origin atom. The last column of the Table 4 shows the detailed vibrational assignment obtained from

**Table 2:** Definition of Internal coordinates of Clioquinol.

| No | Symbol | Type | Definition |
|---|---|---|---|
| 4-1 | v | CH | C7-H17,C2-H14,C3-H15,C4-H16. |
| 13-5 | v | CC | C2-C3,C3-C4,C4-C5,C5-C10,C5-C6, C6-C7,C7-C8,C8-C9,C9-C10. |
| 14 | v | CCL | C6-Cl13. |
| 15 | v | CI | C8-I12. |
| 16-17 | v | NC | N1-C2,N1-C10. |
| 18 | v | CO | C9-O11. |
| 19 | v | OH | O11-H18. |
| 20-25 | β | R1b | N1-C2-C3,C3-C4-C5,C5-C10-N1, C2-C3-C4,C4-C5-C10,C10-N1-C2. |
| 26-31 | β | R2b | C5-C6-C7,C7-C8-C9,C9-C10-C5, C6-C7-C8,C8-C9-C10,C10-C5-C6. |
| 32-33 | β | ICCb | I12-C8-C7, I12-C8-C9 |
| 34-35 | β | CCLb | C7-C6-Cl13, C5-C6-Cl13. |
| 36-37 | β | CCOb | C8-C9-O11, C10-C9-O11. |
| 38 | β | COHb | C9-O11-H18. |
| 39-40 | β | NCHb | N1-C2-H14, C3-C2-H14 |
| 41-46 | β | CCHb | C2-C3-H15, C4-C3-H15, C3-C4-H1, C5-C4-H16, C8-C7-H17, C6-C7-H17. |
| 47 | β | CCNb | C9-C10-N1. |
| 48 | β | CCCb | C4-C5-C6. |
| 49 | γ | ICo | I12-C8-C9-C7. |
| 50-53 | γ | CHo | H15-C3-C2-C4,H16-C4-C3-C5,H14-C2-C3-N1, H17-C7-C6-C8. |
| 54 | γ | OCo | :O11-C9-C10-C8. |
| 55 | γ | CLCo | Cl13-C6-C7-C5. |
| 56-57 | γ | CCo | C5-C10-C9-N1,C4-C5-C6-C10 |
| 58-63 | t | R1t | N1-C2-C3-C4,C3-C4-C5-C10,C5-C10-N1-C2, C2-C3-C4-C5,C4-C5-C10-N1, C10-N1-C2-C3. |
| 64-69 | t | R2t | C5-C6-C7-C8,C7-C8-C9-C10,C9-C10-C5-C6, C6-C7-C8-C9,C8-C9-C10-C5, C10-C5-C6-C7 |
| 70-71 | t | buttfly | C6-C5-C10-N1 , C9-C10-C5-C4 |
| 72-73 | t | COt | C10-C9-O11-H18,C8-C9-O11-H18. |

**Table 3:** Definition of local symmetry coordinates.

| No | Symbol | Definition |
|---|---|---|
| 4-1 | CH | R1,R2,R3,R4 |
| 13-5 | CC | R5,R6,R7,R8,R9,R10,R11,R12,R13 |
| 14 | CCL | R14 |
| 15 | CI | R15 |
| 16-17 | NC | R16,R17 |
| 18 | CO | R18 |
| 19 | OH | R19 |
| 20 | TrigR1b | (β20- β21+ β22- β23+ β24- β25)/√6 |
| 21 | SymR1b | (2β20- β21-β22+2 β23- β24-2β25)/√12 |
| 22 | AsymR1b | (β21- β22+ β24- β25)/√2 |
| 23 | TrigR2b | (β26- β27+ β28- β29+ β30- β31)/√6 |
| 24 | SymR2b | (2β26- β27-β28+2 β29- β30-β31)/√12 |
| 25 | AsymR2b | (β27- β28+ β30- β31)/√2 |
| 26 | ICCb | (y32-y33)/√2 |
| 27 | CCLb | (y34-y35)/√2 |
| 28 | CCOb | (v36-v37)/√2 |
| 29 | COHb | M38 |
| 30 | NCHb | (v39-v40)/√2 |
| 31-33 | CCHb | (v41-v42)/√2, (v43-v44)/√2, (v45-v46)/√2 |
| 34 | CCNb | P47 |
| 35 | CCCb | P48 |
| 36 | ICo | P49 |
| 37-40 | CHo | P50, P51, P52, P53 |
| 41 | OCo | P54 |
| 42 | CLCo | P55 |
| 43-44 | CCo | P56, P57 |
| 45 | TrigR1t | (s58-s59+s60-s61+s62-s63)/√6 |
| 46 | SymR1t | (s58-s60+s61-s63)/√2 |
| 47 | AsymR1t | (-s58+2s59-s60-s61+2s62-s63)/√12 |
| 48 | TrigR2t | (s64-s65+s66-s67+s68-s69)/√6 |
| 49 | SymR2t | (s64-s66+s67-s69)/√2 |
| 50 | AsymR2t | (-s64+2s65-s66-s67+2s68-s69)/√12 |
| 51 | buttfly | (s70-s71)/√2 |
| 52 | COt | (s72-s73)/2 |

the calculated Potential Energy Distribution (PED). The heterocyclic aromatic compounds and its derivatives are structurally very close to benzene. The C-H stretching vibrations [25] of aromatic and hetero aromatic cover in the region of 3100 $cm^{-1}$-3000 $cm^{-1}$. This permits the ready identification of the structure. The frequencies at 3120, 3100 and 3028 $cm^{-1}$ in FT-IR spectrum and 3125, 3105 $cm^{-1}$ in the FT-Raman is assigned to C-H stretching aromatic ring. The C-H bending vibration appears at two distinct regions 1300-1000 $cm^{-1}$ and 700-610 $cm^{-1}$ [26-28]. The bands at 1200, and 953 $cm^{-1}$ in FT-IR and the bands at 1205 and 950 $cm^{-1}$ in the FT-Raman spectrum have been assigned to COH bending vibrations. The vibration belonging to the bond between the ring and the halogen atom are worth to discuss since mixing of vibrations are possible due to the lowering of the molecular symmetry and the presence of heavy atoms on the periphery of the molecule [29] coupling with other groups may result in shift in the absorption band as high as 840 $cm^{-1}$.For simple chlorine containing organic compounds, C-Cl absorption are in the region 750-700 $cm^{-1}$,whereas for the Trans- and Gauche- [30] forms they are near 650$cm^{-1}$ .In the present study, the band observed at 649 $cm^{-1}$ in the IR spectrum and the same band is observed in Gunasekaran *et al.* [27], 650 $cm^{-1}$ in the IR and 652 $cm^{-1}$ in Raman spectrum in Sundaraganesan *et al.* [31] which is identified as C-Cl stretching and CCl bending corresponding to experimental values at 670, 649 $cm^{-1}$ of FTIR and 670, 650 $cm^{-1}$ of FT-Raman in our present study. This mode is not pure but contains significant contribution from other modes. This result is in agreement with reported values given by Varghese *et al.* [32], George *et al.* [33] and Palafox *et al.* [34]. The O–H group vibrations are likely to be the most sensitive to the environment, so they show pronounced shifts in the spectra of the hydrogen-bonded species. With stronger intermolecular bonding, the O-H stretching vibrations may give rise to broad and intense bands which are often overlaid with peaks due to Fermi-resonance interactions. In the present molecule, the band observed at 3218 $cm^{-1}$ in FTIR is assigned to O-H stretching with 98% PED contribution. The O-H in-plane bending vibration for phenols, in general, lies in the region 1150–1250 $cm^{-1}$ and is not much affected due to hydrogen bonding unlike to stretching and out-of-plane bending wave numbers [35]. In both inter-molecular and intra-molecular associations, the wave number is at a higher value than in free O-H. The wave number increases with hydrogen-bond strength because of the large amount of energy required to twist the O-H bond. The C-O-H out-of-plane bending vibration computed by B3LYP/6-21G (d) at 1209,839, $cm^{-1}$ shows good agreement with the recorded FT-IR band at 1200,740 $cm^{-1}$. If a compound contains carbonyl group the absorption caused by C-O stretching is generally strong among the strongest present [36]. Accordingly, the FTIR bands observed at 1270, 1120 $cm^{-1}$ and 1275 $cm^{-1}$ at FT-Raman in clioquinol have been assigned to C-O stretching modes of vibrations. The assignments of C-O in-plane and out-of-plane bending vibrations made in this study are supported by the literature Ashdown and Kletz [37] have reported number of such cases and the range of frequencies 1020 $cm^{-1}$-1110 $cm^{-1}$ associated with the C-O linkage. In the present case, the experimental frequencies at 620 $cm^{-1}$ in FTIR and 615 $cm^{-1}$ in FT-Raman spectrum of clioquinol are assigned to C-C-O asymmetric bending vibrations; this is an excellent agreement with the predicted frequency at 627 $cm^{-1}$.

## Ligand docking

Ligand docking referred to cases where small molecular (ligand) is being docked into much larger macromolecule (target). The interaction between proteins and other molecules is fundamental to all biological functions. This include tools that can assist in prediction of interaction sites on protein surface and tools for predicting the structure of the intermolecular complex formed between two or more molecules (docking). Molecular docking was performed to obtain protein-ligand binding energy and to identify potential ligand binding sites. Docking calculations were carried out with Autodock tools. The 3D structure of clioquinol was generated by PyMol for visualizing the interaction of docked protein-ligand complex. Figure 4 shows (secondary structure) the ligand sites and polar contacts of

**Table 4:** Experimental, computed frequencies ($cm^{-1}$) and PED with assignments of Clioquinol with 6-21G(d).

| MODE No. | IR | RAMAN | HF | B3LYP | Assignments PED% |
|---|---|---|---|---|---|
| 1 | 3218 | - | 3300 | 3200 | vOH ( 98) |
| 2 | 3120 | 3125 | 3280 | 3128 | vCH ( 99) |
| 3 | 3100 | 3105 | 3245 | 3110 | vCH ( 99 |
| 4 | - | - | 3234 | 3090 | vCH ( 99) |
| 5 | 3028 | - | 3210 | 3030 | vCH ( 99) |
| 6 | 1645 | 1640 | 1660 | 1642 | vCC ( 58)+ COHb( 11) |
| 7 | 1604 | 1610 | 1620 | 1602 | vCC( 48)+ CCHb( 21)+ vNC( 15) |
| 8 | 1575 | 1580 | 1580 | 1575 | vCC( 51)+vNC+( 10) |
| 9 | 1540 | 1545 | 1530 | 1520 | CCHb( 49)+ vCC( 40) |
| 10 | 1498 | 1500 | 1490 | 1468 | vCC( 36)+ NCHb( 28)+ vNC( 15) |
| 11 | 1459 | 1463 | 1432 | 1428 | CCHb( 52)+ vCC( 29) |
| 12 | - | - | 1423 | 1413 | vCC( 52)+ COHb( 28) |
| 13 | - | - | 1410 | 1405 | vNC( 28)+ NCHb( 20)+ vCC( 17)+ VCO( 11)+ CCHb( 10) |
| 14 | 1360 | - | 1342 | 1330 | vCC( 56)+ COHb( 20) |
| 15 | - | - | 1284 | 1276 | vNC 20)+ CCHb( 19+ vCC(17)+ NCHb( 16)+ TrigR2(12) |
| 16 | 1270 | 1275 | 1271 | 1264 | vCC(39)+ CCHb( 20)+ VCO( 15)+ vNC( 14) |
| 17 | - | - | 1230 | 1229 | CCHb( 37)+ vCC( 34) |
| 18 | 1200 | 1205 | 1220 | 1209 | vCC( 53)+ vNC( 15)+ COHb( 14) |
| 19 | - | - | 1172 | 1165 | vCC( 42)+ CCHb ( 19)+ vNC( 12)+ TrigR2( 10) |
| 20 | 1120 | - | 1135 | 1104 | vCC( 26)+ TrigR1( 21)+ VCO( 14)+ CCHb( 10) |
| 21 | 1095 | 1090 | 1080 | 1053 | vCC ( 71) |
| 22 | 1050 | - | 1072 | 1041 | CHo( 86)+ TrigR1( 11) |
| 23 | 990 | - | 1000 | 990 | CHo ( 85) |
| 24 | - | - | 991 | 981 | VCCL( 20)+ vNC( 17)+ TrigR1( 15)+ AsymR2( 13)+ TrigR2( 13)+ vCC( 10) |
| 25 | 953 | 950 | 945 | 940 | CHo( 66)+ TrigR2( 21) |
| 26 | - | - | 933 | 921 | TrigR1( 31)+ TrigR2( 26)+ OCo( 14)+ CHo( 13) |
| 27 | 869 | - | 880 | 870 | vCC ( 24)+ TrigR1( 17)+ VCl ( 13)+ SymR1b ( 12) |
| 28 | - | - | 860 | 839 | CHo( 77) |
| 29 | 740 | - | 760 | 747 | COt ( 61)+ OCo ( 15) |
| 30 | - | - | 750 | 732 | vCC( 36)+ AsymR1( 15)+ VCO( 13)+ TrigR2( 11) |
| 31 | - | - | 735 | 728 | OCo( 24)+ TrigR1( 22)+ COt ( 17+, ICo( 10) |
| 32 | 670 | 670 | 685 | 679 | VCCL( 28)+ AsymR2 ( 18)+ SymR1b( 18)+ VCl(16) |
| 33 | 649 | 650 | 650 | 633 | CLCo( 26)+ SymR2t( 25)+ TrigR2( 16) |
| 34 | 620 | 615 | 630 | 627 | AsymR1( 42)+ CCOb( 19) |
| 35 | 563 | 566 | 572 | 569 | vCC( 19)+ CCLb( 19)+ CCCb( 15)+ SymR1b( 14)+ AsymR1 ( 10) |
| 36 | 548 | 550 | 535 | 533 | AsymR2( 24)+ AsymR1( 20)+ ICo( 18)+ SymR1t ( 11) |
| 37 | 510 | 505 | 520 | 516 | SymR2b( 31)+ SymR1b( 15)+ AsymR2( 12)+ vCC(10) |
| 38 | 450 | 445 | 445 | 440 | AsymR1(39)+ SymR1t(16) |
| 39 | 426 | 425 | 394 | 371 | CLCo(29)+ ICo( 21)+ OCo( 19)+ SymR1t( 11) |
| 40 | - | - | 360 | 353 | VCCL( 44) AsymR2( 31)+ vCC 11) |
| 41 | - | - | 302 | 299 | CCOb( 41)+ CCNb( 12)+ CCLb( 11) |
| 42 | - | - | 246 | 226 | AsymR1( 34)+ buttfl( 17)+ ICo( 13) |
| 43 | - | 216 | 235 | 216 | VCl( 22)+ CCLb( 16)+ SymR2b( 15)+ CCCb( 12) |
| 44 | - | - | 187 | 161 | CCLb( 40)+ VCl( 32)+ vCC( 12) |
| 45 | - | 150 | 168 | 158 | SymR1t( 28)+ SymR2t( 22)+ AsymR2( 22)+ TrigR2(11) |
| 46 | - | - | 131 | 128 | CLCo( 28)+ ICo( 23)+ SymR2t( 18) |
| 47 | - | - | 126 | 116 | ICCb( 81) |
| 48 | - | - | 71 | 60 | SymR2t( 46)+ ICo( 15)+ AsymR2 ( 12)+ OCo ( 11) |

Frequency main % contributions to the P.E.D. in symmetry coordinate.

clioquinol. Protein coloured according to secondary structure beta sheets in green, orange, yellow and helices in red, blue, green. The arrows shows the direction of the beta-sheets, which is from the N- and C- terminus. The point in opposite direction shows they are anti-parallel. Apparently, one should note high number of different proteins folds, this is due to number of amino acid sequences. Oxidoreductase as enzyme which is responsible for metabolic process and HIF-1α inhibitor that decreases the enzyme activity. The HET residuces are 1352 $SO_4$ and 1353 $SO_4$, they are the non-standard residuces in the entry.

Figure 5 shows the assessment of the Ramachandran plot (scatter plot) of clioquinol. Ramachandran plot is a way to visualize dihedral

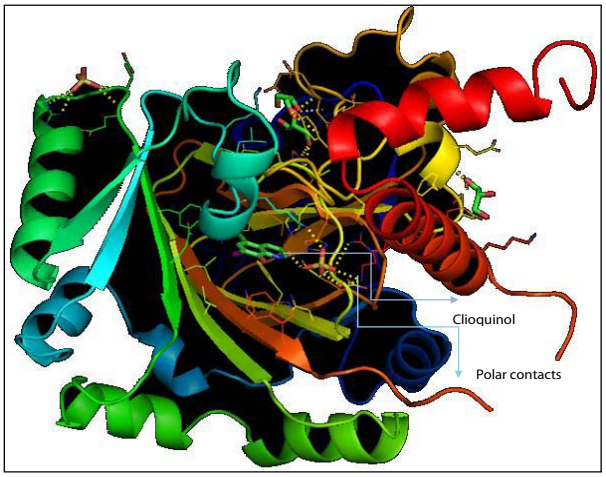


**Figure 4:** Secondary structure of Clioquinol.

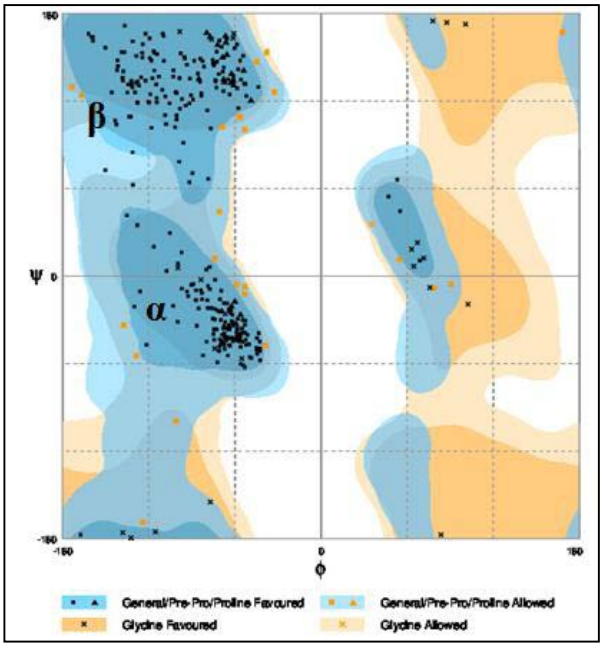


**Figure 5:** Ramachandran plot of Clioquinol.

angles ψ against Φ of amino acid residuces in protein structure. The two torsion angles of the polypeptide chain describe the rotations of poplypeptide backbone around the bonds between N-Cα (Φ) and Cα-C(ψ). We tried to show the conformation of the Φ and ψ angles are possible for an amino acid residue in a protein. One can observe from the Figure 5, the darkest areas correspond to the "core" regions representing the most favourable combinations of Φ and ψ values. This "core" region guides to stereo chemical quality and thus it shows both the proline and glycine favoured and allowed regions. It is clearly being seen on the scatter plot, on the plot the region marked α is for α-helices and β is for beta sheet. Each dot on the plot provides the ψ and Φ values for an amino acid in a protein. The regions on the plot with the highest density of dots are the allowed regions (low-energy regions).

## Electronic Properties

The Frontier molecular orbital plays an important role in the electric and optical properties and chemical reaction [38]. Many organic molecules that containing conjugated π electrons are characterized hyperpolarizabilities and were analyzed by means of vibrational spectroscopy [39,40]. In most cases, even in the absence of inversion symmetry; the strongest bands in the Raman spectrum are weak in the IR spectrum and vice-versa. But the intramolecular charge transfer from the donor to acceptor group through a single-double bond conjugated path can induce large variations of both the molecular dipole moment and the molecular polarizability, making IR and Raman activity strong at the same time. The analysis of the wave function indicates that the electron absorption corresponds to the transitions from the ground to the first excited state and is mainly described by one-electron excitation from the Highest Occupied Molecular Orbital (HOMO) to the Lowest Unoccupied Molecular Orbital (LUMO) Figure 6. shows the atomic orbital HOMO- LUMO composition of the frontier molecular orbital computed at the DFT (B3LYP) with 6-21G (d) basis of clioquinol. The calculations indicate that the title compound has (72) occupied molecular orbital. The positive phases are red and the negative ones are green. As seen from the Figure 6 in HOMO, the electrons are mainly localized on the chlorine and quinoline ring (donor). However, when electron transition takes place, some electron will enter into LUMO, and then the electron will mainly be localized on quinoline ring (acceptor). Namely, electron transitions are corresponding to the π→π*. The HOMO-LUMO energy gap of clioquinol was calculated at the B3LYP/6-21G (d) level reveals that the energy gap reflects the chemical activity of the molecule. HOMO energy = -5.9631 eV, LUMO energy = -1.9459 eV, HOMO-LUMO energy gap = 4.017 eV.

### Natural bond orbital analysis

Natural Bond Orbital analysis performs the analysis of a many-electron molecular wave function in terms of localized electron-pair "bonding' units. The analysis is based on a method for optimally transforming a given wavefunction into localized form, corresponding to the one-center (lone pair) and two-center (bond) elements of the chemist's lewis structure picture. The second-order Fock matrix was carried out to evaluate the donor-acceptor interactions in NBO analysis. The interactions' result is the loss of occupancy from the localized NBO of the idealized Lewis structure into an empty non-Lewis orbital. For each donor (i) and acceptor (j), the stabilization

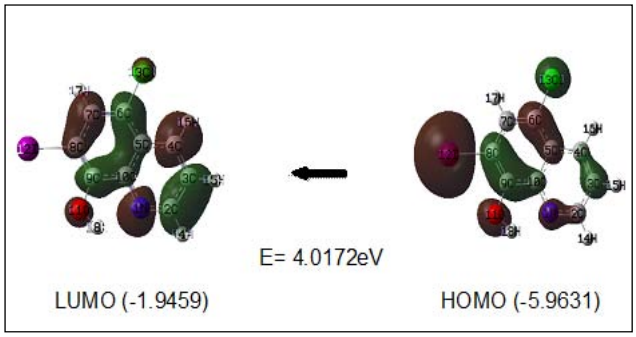


**Figure 6:** Atomic orbital HOMO – LUMO composition of the frontier molecular orbital for Clioquinol.

**Table 5:** Second Order Perturbation Theory Analysis of Fock Matrix in NBO Basis.

| Donor NBO(i) | Type | ED/e | Acceptor NBO(j) | Type | ED/e | [a]E(2) Kcal/mol | [b]E(j)-E(i) a.u. | [c]F(i,j) a.u. |
|---|---|---|---|---|---|---|---|---|
| N 1 – C 2 | π | 1,8175 | C 5 – C 10 | π* | 0.9704 | 22.29 | 0.37 | 0.088 |
| C 2 - C 3 | σ | 1.9579 | C 3 - C 4 | σ* | 0.0536 | 28.45 | 2.21 | 0.225 |
| C 4 - C 5 | σ | 1.9326 | C 3 - C 4 | σ* | 0.0536 | 21.19 | 2.18 | 0.192 |
| C 5 - C 10 | π | 1.5871 | C 8 - C 9 | π* | 0.408 | 25.48 | 0.3 | 0.079 |
| C 6 - C 7 | π | 1.7223 | C 5 - C 10 | π* | 0.9704 | 22.75 | 0.32 | 0.081 |
| C 8 - C 9 | π | 1.6858 | C 6 - C 7 | π* | 0.569 | 25.26 | 0.31 | 0.08 |
| N 1 - C 2 | π* | 0.2456 | C 5 - C 10 | π* | 0.9704 | 137.32 | 0.03 | 0.091 |
| C 5 - C 10 | π* | 0.4704 | C 3 - C 4 | π* | 0.141 | 25.04 | 0.15 | 0.099 |
| C 6 - C 7 | π* | 0.5695 | C 5 - C 10 | π* | 0.9704 | 271.19 | 0.02 | 0.091 |
| C 8 - C 9 | π* | 0.408 | C 5 - C 10 | π* | 0.9704 | 262.4 | 0.02 | 0.096 |

[a]E (2) means energy of hyper conjugative interaction (stabilization energy).
[b]Energy difference between donor and acceptor i and j NBO orbitals.
[c]F (i, j) is the fock matrix element between i and j NBO orbitals.

energy E (2) associated with the delocalization i→j is estimated as $E_2 = \Delta E_{ij} = q_i (F(i.j)^2 / (\varepsilon_j - \varepsilon_i))$.

Where $q_i$ is the donor orbital occupancy, $\varepsilon_j$ and $\varepsilon_i$ are diagonal elements and F (i, j) is the off diagonal NBO Fock matrix element. The second order perturbative estimates of 'donor-acceptor' (bond-antibond) interactions in the NBO basis. From the Table 5, Interestingly, the NBO analysis clearly manifests the evidence of the ICT from π*(C6-C7)- π*(C5-C10) , π* to π*(N1-C2) to (C5-C10) and π* to π* (C8-C9) to (C5-C10) with large stabilization energy of 271, 137 and 262kcal/mol.

## Conclusion

Density functional theory calculations have been carried out on the structure and vibrational spectrum of clioquinol. The equilibrium geometry computed by B3LYP method for both the bond angles and bond lengths are performed better. The vibrational frequency analysis of some values DFT method agrees satisfactorily with experimental results. On the basis of agreement between the calculated and experimental results, assignment of all the fundamental vibrational modes of clioquinol were examined and proposed in this investigation. The PED contributions to each of the observed frequencies show the reliability and accuracy of the spectral analysis. This study demonstrates that scaled DFT/B3LYP calculations are a powerful approach for understanding the vibrational spectra of medium sized organic compounds. Further employment of molecular docking to find ligand sites of clioquinol are favourable for structure based drug design.

## References

1. Rohde W, Mikelens P, Jackson J, Blackman J, Whitcher J, Levinson W. Hydroxyquinolines inhibit ribonucleic acid-dependent deoxyribonucleic acid polymerase and inactivate Rous sarcoma virus and herpes simplex virus. Antimicrob Agents Chemother. 1976; 10: 234-240.
2. Nguyen T, Hamby A, Massa SM. Clioquinol down-regulates mutant huntingtin expression in vitro and mitigates pathology in a Huntington's disease mouse model. Proc Natl Acad Sci USA. 2005; 102: 11840-11845.
3. Ritchie CW, Bush AI, Mackinnon A, Macfarlane S, Mastwyk M, MacGregor L, et al. Metal-protein attenuation with iodochlorhydroxyquin (clioquinol) targeting Abeta amyloid deposition and toxicity in Alzheimer disease: a pilot phase 2 clinical trial. Arch Neurol. 2003; 60: 1685-1691.
4. Chen D, Cui QC, Yang H, Barrea RA, Sarkar FH, Sheng S, et al. Clioquinol, a therapeutic agent for Alzheimer's disease, has proteasome-inhibitory, androgen receptor-suppressing, apoptosis-inducing, and antitumor activities in human prostate cancer cells and xenografts. Cancer Res. 2007; 67: 1636-1644.
5. Ding WQ, Liu B, Vaught JL, Yamauchi H, Lind SE. Anticancer activity of the antibiotic clioquinol. Cancer Res. 2005; 65: 3389-3395.
6. Ming Guo, Wei-Jun Lu, Ping-Gui Yi, Qing-Sen Yu. Study on the thermodynamic characteristics between fluoroquinolone and bovine serum albumin. J Chem Thermodyn. 2007; 39: 337-343.
7. Lu Y, Wang G, Lu X, Lv J, Xu M, Zhang W. Molecular mechanism of interaction between norfloxacin and trypsin studied by molecular spectroscopy and modeling. Spectrochim Acta A Mol Biomol Spectrosc. 2010; 75: 261-266.
8. Skauge T, Turel I, Sletten E. Interaction between ciprofloxacin and DNA mediated by $Mg^{2+}$-ions. Inorg Chim Acta. 2002; 339: 239-247.
9. Hess BA, Schaad J, Carsky P, Zahradnik R. Chem Rev. 1986; 86: 709-730.
10. Pulay P, Zhon X, Fogarasi G. in NATO ASI Seris. (Ed. RFransto), Kluwer: Dordrecht C. 1993; 406: 99-100.
11. Andzelm J, Wimmer E. J Chem Phys. 1992; 96: 1280-1285.
12. Becke AD. J Chem phys. 1992; 96: 2155-2160.
13. Onhson BJ, Gill PMW, Pople JA. Chem Phys. 1993; 98: 5612-5613.
14. Nicholas C Handy, Christopher W Murray, Roger D Amos. Study of methane, acetylene, ethene, and benzene using Kohn-Sham theory. J Phys Chem. 1993; 97: 4392-4396.
15. Delano P Chong, Alan V Bree. Calculated infrared intensities for the bending mode in some small linear molecules. Chem phys let. 1993; 210: 443-447.
16. Berces A, Zeigler T. J chem Phys. 1993; 98: 4793-4803.
17. Fiona Sim, Alain St Amant, Imre Papai, Dennis R Salahub. Gaussian density functional calculations on hydrogen-bonded systems. J Am chem Soc. 1992; 114: 4391-4400.
18. Nicholas C Handy, Paul E Maslen, Roger D Amos, Jamie S Andrews, Christopher W Murray, Gregory J Laming. The harmonic frequencies of benzene. Chem phys let. 1992; 197: 506-515.
19. Ramachandran KI, Deepa G, Namboori K. Computational Chemistry and Molecular Moldeling Principles and Applications, Springer-Verlag Berlin Heidelberg. 2008.
20. Stephens PJ, Devlin FJ, Chavalowski CF, Frish M. Ab Initio Calculation of Vibrational Absorption and Circular Dichroism Spectra Using Density Functional Force Fields: A Comparison of Local, Nonlocal, and Hybrid Density Functionals. J phys chem. 1995; 99: 16883-16902.
21. Frisch MJ, Trucks GW, Schlegel HB, Scuseria GE, Robb MA, Cheeseman JR, et al. Gaussian Inc. Waling ford, CT. 2004.
22. Schlegel HB. Optimization of equilibrium geometries and transition structures. J Comput Chem. 1982; 3: 214-218.

23. Sundius T. Molvib - A flexible program for force field calculations. J Mol Struct. 1990; 218: 321-326.

24. Moon H, Han S, Park H, Choe J. Crystal structures of human FIH-1 in complex with quinol family inhibitors. Mol Cells. 2010; 29: 471-474.

25. Casini A. X-ray Crystallograpy of the Antiepileptic Drug Zonisamide with CA II. Acta Cryst. 2005; 61: 242-243.

26. Arivazhagan M, Joseph Prince J, Balachandran V. FTIR and FT-Raman spectral investigation of 2-chloro-l, 3-dibromo-5- fluorobenzene. Ind J pure and applied Physics. 2008; 46: 698-701.

27. Gunasekaran S, Natarajan RK, Shyamala D, Rathika R. Normal coordinate analysis of urea meta nitro benzoic acid crystal. Ind J pure and applied Phys. 2006; 44: 315-319.

28. Krishnakumar V, John Xavier R. Chem Phys. 2005; 312: 227-240.

29. Chengteh Lee, Weitao Yang, Robert G Parr. Development of the Colle-Salvetti correlation-energy formula into a functional of the electron density. Phys Rev. 1988; 37: 785-786.

30. Socrates G. "Infrared characteristics group frequencies", John Wiley, NewYork. 1987.

31. Sundaraganesan N, Joshua BD, Rajamoorthy M, Gangadhar CH. FT-IR, FT-Raman spectra and ab- initio DFT vibrational analysis of 2-chloro-5-aminopyridine. Ind J pure and appl Phys. 2007: 45; 969-978.

32. Varghese HT, Panicker CY, Philip D, Pazdera P. Vibrational spectroscopic studies and ab initio calculations of 2-cyanophenylisocyanid dichloride. Spectrochim Acta A Mol Biomol Spectrosc. 2007; 67: 1055-1059.

33. George WO, S. Mcintyre S. "Introduction to Spectroscopy" John Wiley, New York. 1987.

34. Palafox MA, Rastogi VK, Mittal L. Benzonitriles: Survey of their importance and scaling of their vibrational frequencies. Int J. Quantum Chem. 2003; 94: 189-204.

35. Varsanyi G. "Assignments for vibrational spectra of seven hundred Benzene Derivatives". Wiley, New York. 1973.

36. Sathyanarayana DN. "Vibrational spectroscopy-Theory and applications" New age International. New delhi. 2004.

37. Ashdown A, Kletz TA. J chem Soc. 1948; 1039: 1454-1456.

38. Fleming I. Frontier orbital and Organic Chemical Reactions, Wiley, London. 1976.

39. Ataly Y, Avci D, Basoglu A. Struct Chem. 2008; 19: 239- 246.

40. Vijayakumar T, Hubert Joel I, Nair CPR, Jayakumar VS. Efficient π electrons delocalization in prospective push–pull non-linear optical chromophore 4-[N,N-dimethylamino]-4′-nitro stilbene (DANS): A vibrational spectroscopic study. Chem Phys. 2008; 343: 83-99.